Available online at www.sciencedirect.com
ScienceDirect
Trans. Nonferrous Met. Soc. China 34(2024) 2881−2888
Transactions of Nonferrous Metals Society of China
www.tnmsc.cn

Versatile fluidity test model for cast superalloys and comparison between IN718 and IN939

Jun ZHANG[1], Zi-qi JIE[2], Miao-nan LIU[1], Min GUO[1]

1. State Key Laboratory of Solidification Processing, Northwestern Polytechnical University, Xi'an 710072, China;
2. School of Materials Science and Chemical Engineering, Xi'an Technological University, Xi'an 710021, China

Received 29 March 2023; accepted 10 August 2023

Abstract: A spiral fluidity test model of superalloys with 10 mm in height and 3 mm in thickness was designed to evaluate the fluidity of two distinct Ni-based superalloys IN718 and IN939. The factors influencing fluidity are ascertained through comparative analysis utilizing methodologies such as JMatPro, differential scanning calorimetry and high-temperature confocal laser scanning microscopy. The results show that under identical testing conditions, the fluidity of the IN939 superalloy surpasses that of the IN718 superalloy. When subjected to the same temperature, the melt viscosity and surface tension of IN939 superalloy are considerably reduced relative to those of IN718 superalloy, which is beneficial to improving the melt fluidity. Furthermore, the liquidus temperature and solidification range for the IN939 superalloy are both smaller compared with those of the IN718 superalloy. This condition proves advantageous in delaying dendrite coherency, thereby improving fluidity.

Key words: fluidity; solidification range; superalloys; surface tension; viscosity

1 Introduction

Ni-based superalloys are extensively utilized in core components of aeroengines and industrial gas turbines, primarily owing to their exceptional strength, and superior creep and corrosion resistance at high temperatures [1,2]. As engine performance advances, the demand for larger, more intricate, and thin-walled castings, such as cases, nozzles, and cartridges grows, thereby rendering difficulty in simultaneously controlling the filling and cooling processes in investment casting [3,4]. Concurrently, the addition of more refractory elements endows the superalloys with high viscosity and a wide solidification temperature range, which can result in significant defects, reduced yield, and compromised performance [5−7].

The fluidity of the alloy melt, indicative of its castability, serves as fundamental data for designing the casting process and significantly influences filling ability and solidified microstructure of the casting. High fluidity ensures complete mold filling and exceptional dimensional accuracy during the casting formation process, while mitigating casting defects such as cold shuts and shrinkage cavities. Additionally, improved fluidity allows for a reduction in pouring temperature, thus promoting grain refinement. Extensive research indicates that fluidity is dictated primarily by melt features, including composition, temperature, purity, and thermal history [8−13]. The interaction between the melt and the mold also plays a crucial role in fluidity [14].

Fluidity is traditionally measured by the length of the sample formed in a designated test model after melt solidification [8]. Currently, numerous test models, including spiral, radial, step-shaped,

Corresponding author: Zi-qi JIE, Tel: +86-13629245501, E-mail: jzq603@163.com
DOI: 10.1016/S1003-6326(24)66582-9
1003-6326/© 2024 The Nonferrous Metals Society of China. Published by Elsevier Ltd & Science Press
This is an open access article under the CC BY-NC-ND license (http://creativecommons.org/licenses/by-nc-nd/4.0/)

octopus, U-type, and various derivatives, are popularly used [8−13,15−24]. With the development of a mathematical model for liquid metal ground in thermophysical parameters, solidification characteristics, and transport processing, fluidity can be theoretically predicted and characterized using simulation software [25−29].

However, there are at least two important issues that require further exploration concerning superalloy fluidity. First, current fluidity test models are designed primarily for low-melting-point alloys under non-vacuum conditions, thus rendering them inappropriate for superalloys with high melting points, viscosities, and chemical activities. Additionally, the accuracy and applicability of the calculated data are questionable owing to the severe scarcity of thermophysical parameters for superalloys. Second, fluidity evaluations for superalloys are fundamentally empirical owing to insufficient research on melt flow characteristics, particularly for different types of superalloys. Further, comparative fluidity data for various conditions are limited.

In this study, a standard, versatile fluidity test model for superalloys was proposed under vacuum conditions. The fluidity of two prominent and extensively utilized Ni-based superalloys, IN718 and IN939, was evaluated using this novel test model. To elucidate the difference between the two alloys, thermophysical properties were computed using JMatPro software, solidification characteristics were examined using differential scanning calorimetry (DSC), and the solidification process was observed in-situ via high-temperature confocal laser microscopy (HLCLSM). Thus, this work aimed to provide a versatile standardized method for superalloy fluidity testing and assessment, which may be beneficial to the design of investment casting techniques.

2 Experimental

2.1 Materials

The IN718 and IN939 superalloys utilized as experimental materials in this study have been implemented in large and complex castings in aeroengines owing to their impressive castability and mechanical properties. The chemical compositions of both alloys are detailed in Table 1. IN939 is a γ' phase-strengthened nickel-based superalloy boasting a service temperature around 850 ºC and superior corrosion resistance, essentially surpassing the quality of IN718, which is predominantly strengthened by the γ'' phase. Thermophysical properties, such as viscosity, surface tension, specific heat, and latent heat of the superalloys, were calculated employing the JMatPro software.

2.2 Fluidity test model

The proposed spiral fluidity test model is shown in Fig. 1. A small-sized model is advantageous for testing under vacuum conditions. Herein, the flow channel of the model was designed as an asymptote expanding along the radial direction with the gate at the center, and the maximum running length was 980 mm [30].

All wax patterns illustrated in Fig. 1(a), utilized in this study, were prepared by laser prototyping with polystyrene powders. The various layers of the model shell were composed of a mixture of silica-sol and fused mullite in differing proportions. Following the drying process, the model shell underwent dewaxing in an electric furnace, ultimately producing the ceramic mold for the fluidity test (Fig. 1(b)).

2.3 Fluidity test

The influence of the pouring temperature on fluidity was examined using a vacuum induction melting furnace, melting each 1 kg batch of alloy ingot under 0.5 Pa. The parameters for the fluidity test comprised a mold preheating temperature of 900 °C and pouring speed of 0.5 kg/s. Each experiment was conducted at least thrice under these consistent conditions.

2.4 DSC analysis

DSC tests were performed using a NETZSCH

Table 1 Chemical compositions of IN718 and IN939 superalloys (wt.%)

Alloy	Cr	Mo	Al	Ti	Ta	W	Nb	Fe	Co	C	Zr	B	Ni
IN718	18.9	3.1	0.57	0.92	0.005	0.05	5.03	18.91	0.005	0.05	0.014	0.0027	Bal.
IN939	22.48	−	1.88	3.65	1.4	2.01	1.0	−	18.96	0.16	0.10	0.014	Bal.

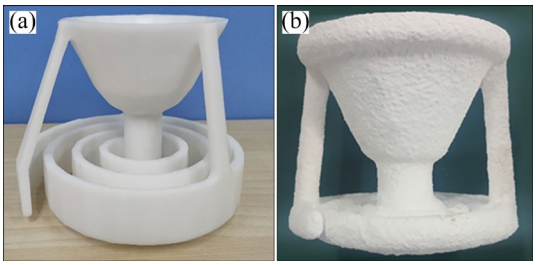

Fig. 1 Wax pattern (a) and ceramic mold (b) for fluidity test

STA 449F3 to ascertain the solidification characteristic temperatures. The DSC samples, weighing approximately 30 mg, were first heated from room temperature to 900 °C at a rate of 20 °C/min, then to 1500 °C at a rate of 10 °C/min. After holding at 1500 °C for 1 min, the samples were cooled to 900 °C at a rate of 10 °C/min. All tests were performed in high-purity alumina crucibles under an argon atmosphere.

2.5 In-situ observation of solidification processing

In-situ observation of solidification processes by HTCLSM offers invaluable firsthand-information on fluidity. The HTCLSM experiments were performed using a VL2000DX-SVF18SP. Cylindrical samples of *d*7.5 mm × 3.0 mm were polished and placed into high-purity alumina crucibles under an ultra-pure argon atmosphere. Helium gas was served as an auxiliary cooling agent during solidification. The sample was heated to 1400 °C at a rate of 60 °C/min, held for 2 min, then cooled to 1000 °C at 50 °C/min, and subsequently cooled to room temperature with the furnace being turned off. The entire process was recorded in real time through both video and photographic means.

3 Fluidity test results

3.1 Design of fluidity test model for superalloys

By referencing the recommended or critical minimum wall thickness of superalloy investment casting, the spiral thickness that is a key parameter affecting the flow length was analyzed. For thin-walled casting, the critical wall thickness can be expressed using the following equation [31]:

$$\delta_c = \sqrt{\frac{\sigma}{\rho g}} \quad (1)$$

where δ_c represents the critical wall thickness; σ denotes the surface tension; ρ stands for the alloy density; g represents the acceleration due to gravity.

Given that the critical wall thickness for most Ni-based superalloys falls below 4.5 mm as per Eq. (1), the selected spiral thicknesses were 3 and 4 mm, respectively. Four fluidity test models, each with varying spiral heights and thicknesses, were designed as depicted in Fig. 2. Models 1 and 2 both featured spiral heights of 25 mm, and thicknesses of 3 and 4 mm, respectively. Model 3 boasted a gradually decreasing spiral height, transitioning from 25 to 10 mm, with a thickness of 4 mm. By contrast, Model 4 displayed a spiral height of 10 mm and thickness of 3 mm.

Table 2 and Fig. 3 present the flow length for IN939 superalloy across the four fluidity test models under the same test conditions. Evidently, Model 2

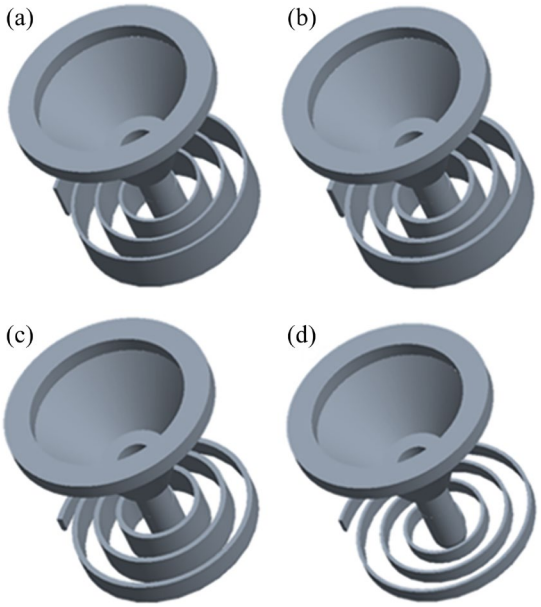

Fig. 2 Fluidity test models: (a) Height 25 mm, thickness 3 mm; (b) Height 25 mm, thickness 4 mm; (c) Height 25−10 mm, thickness 4 mm; (d) Height 10 mm, thickness 3 mm

Table 2 Statistical data of flow length measurements in four fluidity test models for IN939 superalloy

Model	Average length/mm	Standard deviation/%
1	321	16.4
2	819	22.5
3	732	7.15
4	425	8.32

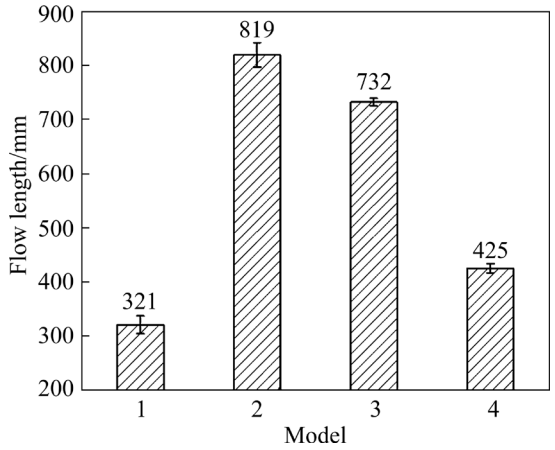

Fig. 3 Flow length of four fluidity test models for IN939 superalloy

demonstrated the maximum flow length, closely followed by Model 3, whereas Model 1 registered the minimal flow length. This can be attributed primarily to the reduced flow resistance of the alloy melt arising from the increased thickness of the mold cavity [23].

The standard deviations in Table 2 illustrate that the data dispersions of flow length in Models 1 and 2 exceeded 10%, whereas those of Models 3 and 4 remained below 10%, indicating that the measured values for Models 3 and 4 are more reliable [20,24]. This can be chiefly attributed to the elevated mold cavity of Models 1 and 2, potentially leading to noticeable shrinkage at the flow end where the melt ceases to flow and solidifies simultaneously (Fig. 4(a)). When the mold cavity height is diminished, as seen in Models 3 and 4, the flow end reverts to its standard shape without shrinkage (Figs. 4(b, c)), suggesting that Models 3 and 4 are more appropriate for evaluating superalloy fluidity.

To expand the test range of fluidity, fluidity must be characterized with the shortest flow length. Consequently, considering the test range, reproducibility, and convenience, Model 4, with a spiral height of 10 mm and spiral thickness of 3 mm was chosen as the standard test model. Using flow length as the evaluation criteria, this model is simple, practical, reliable, and reproducible.

3.2 Fluidity comparison between IN718 and IN939

Figure 5 displays the measured flow lengths (L_f) of the IN718 and IN939 superalloys at various pouring temperatures using Model 4. Evidently, the fluidity of the IN939 superalloy surpasses that of the IN718 superalloy at an equivalent pouring temperature. As the pouring temperature increased from 1400 to 1500 °C, the flow length of the IN939 superalloy was 2.2%−12% longer than that of the IN718 superalloy, and a linear relationship was observed between flow length and pouring temperature.

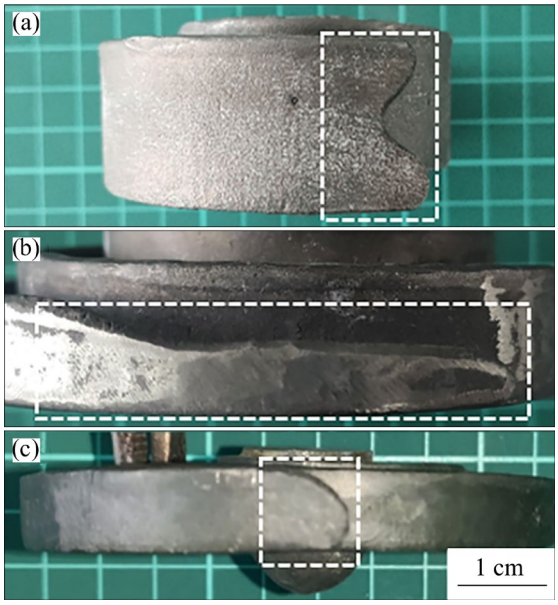

Fig. 4 Shape of flow end for different models: (a) Model 1; (b) Model 3; (c) Model 4

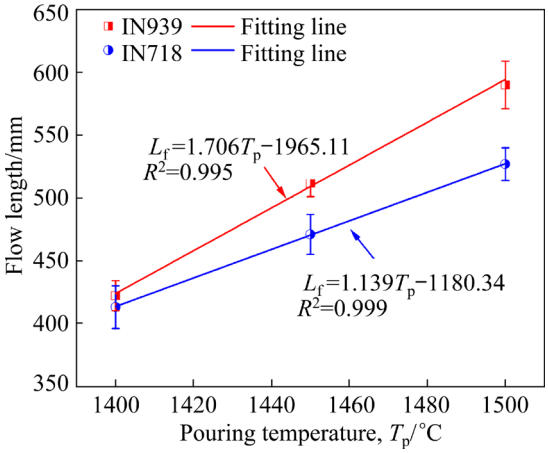

Fig. 5 Flow length of IN718 and IN939 superalloys at different pouring temperatures

4 Discussion

4.1 Thermophysical properties related to fluidity

Figure 6 presents the melt thermophysical properties of the IN718 and IN939 superalloys obtained by the JMatPro calculation. Evidently, IN939 alloy maintains lower viscosity and surface

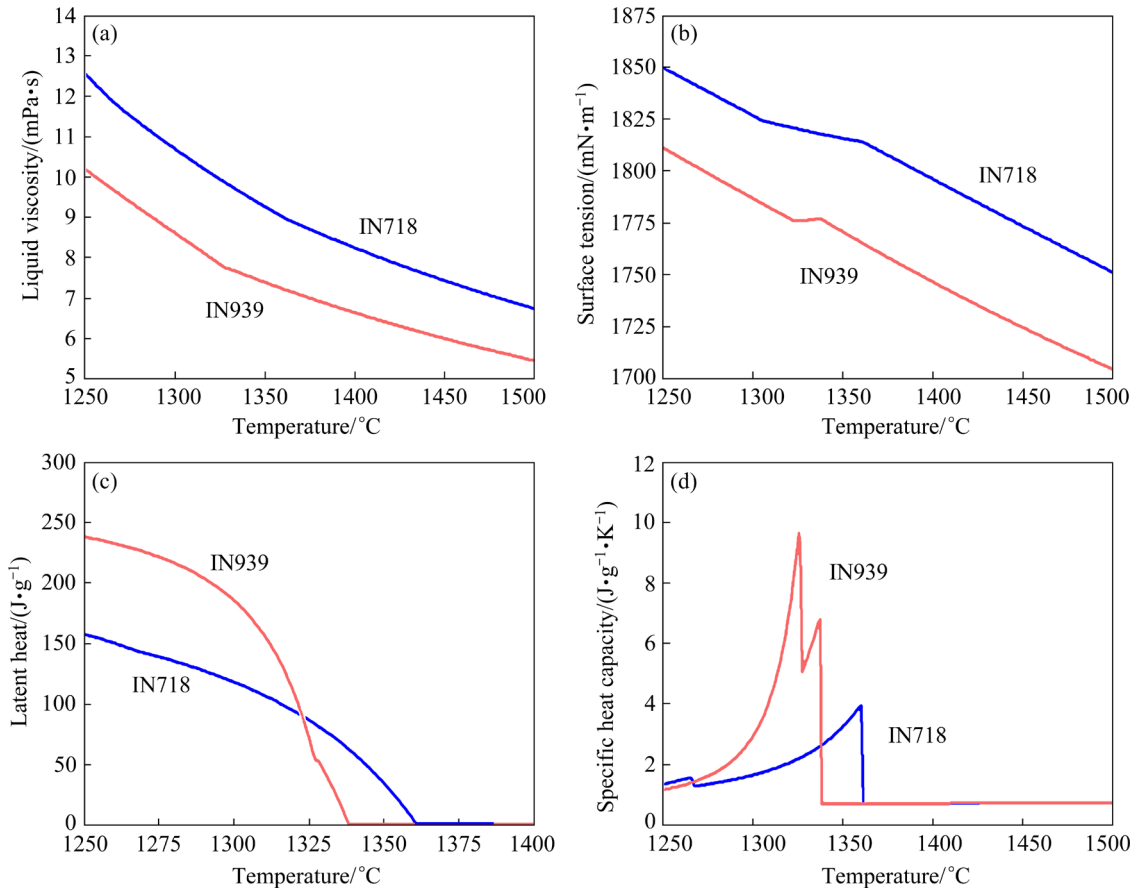

Fig. 6 JMatPro calculation results for IN718 and IN939 superalloys: (a) Viscosity; (b) Surface tension; (c) Latent heat; (d) Specific heat capacity

tension than IN718 alloy, although both viscosity and surface tension decline with increasing melt temperature (Figs. 6(a, b)). Simultaneously, the latent heat and specific heat capacity of the two alloys exhibit significant difference (Figs. 6(c, d)). In comparison to IN718, the IN939 superalloy exhibits higher latent heat below 1322 °C (Fig. 6(c)) and higher specific heat capacity peak below 1337 °C (Fig. 6(d)).

Intuitively, a reduction in surface tension and viscosity may increase the melt flow rate, thereby enhancing fluidity, whereas an increase in latent heat and specific heat capacity may prolong the solidification time, further improving fluidity [20]. Thus, the melt thermophysical properties collectively promote superior fluidity for the IN939 superalloy.

4.2 Solidification characteristics related to fluidity

The liquidus temperature and solidification range considerably influence fluidity [15,19,20]. From the DSC measurement results depicted in Fig. 7, the liquidus temperatures, solidus temperatures, and solidification ranges of the IN718 and IN939 superalloys can be summarized in Table 3. Evidently, IN939 alloy boasts a lower liquidus temperature and solidification range compared with IN718 alloy. Under identical test conditions, a lower liquidus temperature results in high superheat, which can extend the melt flow time [15,19,20]. Furthermore, numerous researchers [15,16,18−20,29] have reported that the solidification range is inversely proportional to the melt fluidity.

The solidification process was observed in situ via high-temperature confocal laser scanning microscopy (HTCLSM), as illustrated in Fig. 8. As the temperature decreased, the melt began nucleation and the formation of dendrites. Once the melt is fully solidified, dendrites become prominently visible (Figs. 8(d, h)). Evidently, the temperature at which the solid phase begins to precipitate in IN718 (1334.1 °C) is higher than that in IN939 (1327.9 °C), thus signifying a delay in the precipitation of the solid phase. Additionally, complete

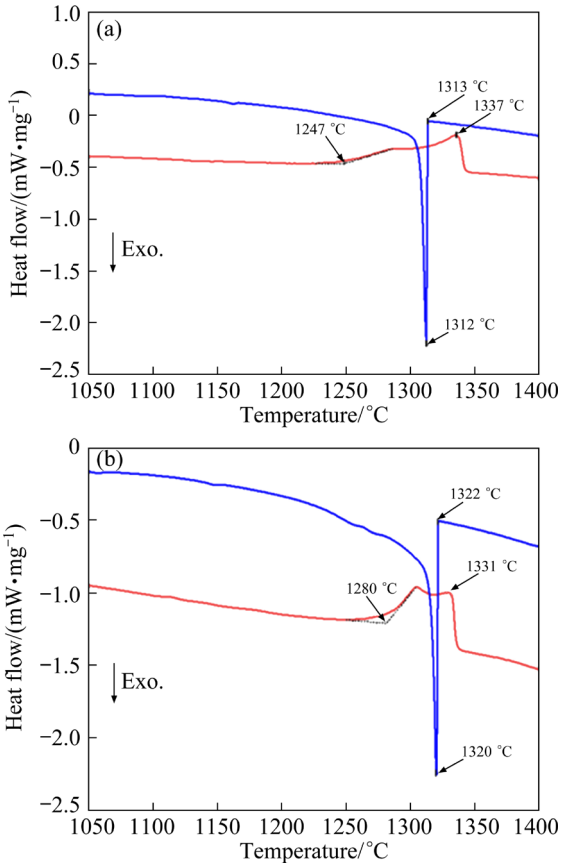

Fig. 7 DSC curves of IN718 (a) and IN939 (b) superalloys

Table 3 Solidification characteristic temperatures of IN718 and IN939 superalloys

Alloy	Liquidus temperature/°C	Solidus temperature/°C	Solidification range/°C
IN718	1337	1247	90
IN939	1331	1280	51

dendrite development is achieved at 1223.3 °C for IN718 (Fig. 8(d)) and 1232.5 °C for IN939 (Fig. 8(h)).

Owing to the wide solidification range, a dendrite network may form when a certain degree of solid phase appears in the superalloy melt during solidification. This dendrite network obstructs the melt flow, thus resulting in increased melt viscosity. Typically, when the solid fraction reaches 20%−40% at the dendrite coherency temperature, the dendrites intersect, thereby arresting the melt flow [8,15]. Based on the HTCLSM results, Fig. 9 depicts the relationship between the liquid fraction and temperature. As the melt temperature decreases, the liquid fraction of both alloys also declines. At the

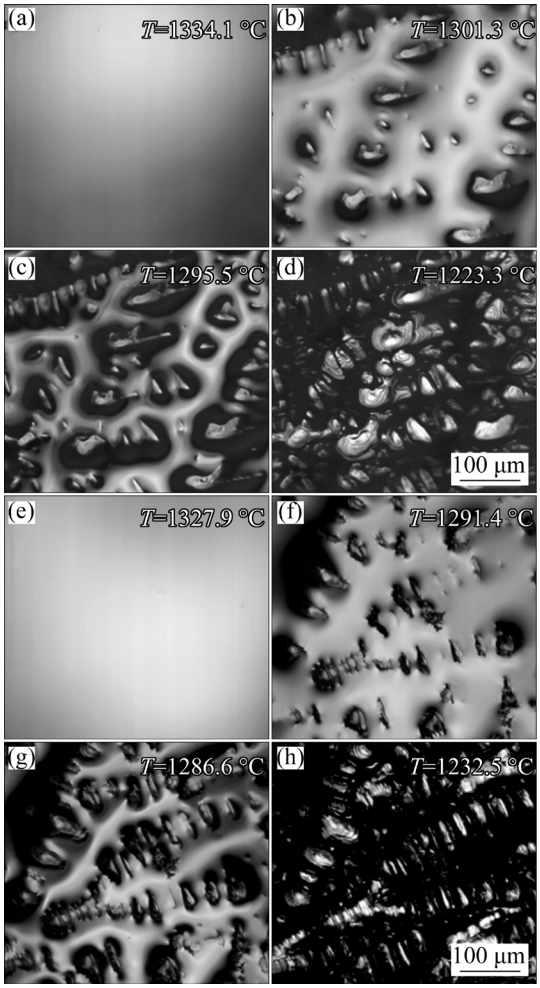

Fig. 8 In-situ observation for solidification process of two superalloys: (a−d) IN718; (e−h) IN939

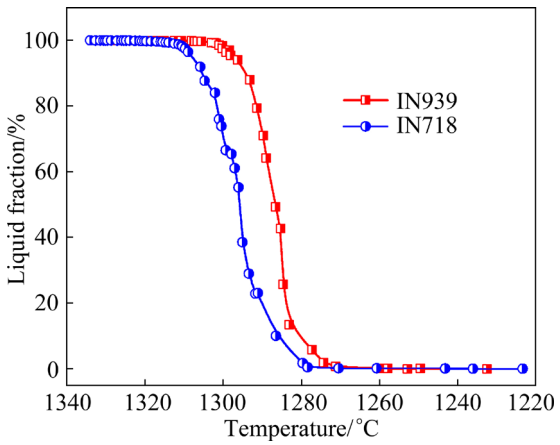

Fig. 9 Curves of liquid fraction as function of melt temperature

same melt temperature, the IN939 superalloy presents a higher liquid fraction than the IN718 superalloy. Figure 9 reveals a substantial difference in the melt temperature between IN718 and IN939

superalloys when the solid fraction attains 40%. Hence, the aforementioned experimental results and analyses suggest that the inherent solidification characteristics also contribute to superior fluidity for the IN939 superalloy.

5 Conclusions

(1) A spiral fluidity test model, specifically tailored for superalloys, was designed with a height of 10 mm and a thickness of 3 mm. The test model utilizes flow length as the primary evaluation criterion, thus offering simplicity, practicality, reliability, and repeatability in its application.

(2) As the pouring temperature increases, the fluidity of the alloy increases. When the pouring temperature increases from 1400 to 1500 °C, the flow length of the IN939 superalloy is observed to be 2.2%−12.0% longer than that of the IN718 superalloy. Moreover, a linear relationship between the flow length and pouring temperature is observed.

(3) The IN939 superalloy exhibits superior fluidity compared with the IN718 superalloy. This advantage is attributed primarily to the inherent thermophysical properties and solidification characteristics of the IN939 superalloy.

CRediT authorship contribution statement

Jun ZHANG: Funding acquisition, Supervision, Resources, Conceptualization, Writing − Reviewing and editing; **Zi-qi JIE:** Investigation, Methodology, Data curation, Writing − Original draft preparation; **Miao-nan LIU:** Investigation, Visualization, Data curation; **Min GUO:** Writing − Reviewing and editing, Supervision.

Declaration of competing interest

The authors declare that they have no known competing financial interests or personal relationships that could have appeared to influence the work reported in this paper.

Acknowledgments

The authors acknowledge the support from the National Natural Science Foundation of China (Nos. 52031012, 51904218).

References

[1] REED R C. The superalloys fundamentals and applications [M]. Cambridge, UK: Cambridge University Press, 2006.

[2] SATISH G J, GAITONDE V N, KULKARNI V N. Traditional and non-traditional machining of nickel-based superalloys: A brief review [J]. Materials Today: Proceedings, 2021, 44: 1448−1454.

[3] WANG Dong-hong, SUN Feng, SHU Da, CHEN Jing-yang, XIAO Chen-bo, SUN Bao-de. Data-driven design of cast nickel-based superalloy and precision forming of complex castings [J]. Acta Metallurgica Sinica, 2022, 58(1): 89−102. (in Chinese)

[4] ZHANG Jun, JIE Zi-qi, HUANG Tai-wen, YANG Wen-chao, LIU Lin, FU Heng-zhi. Research and development of equiaxed grain solidification and forming technology for nickel-based cast superalloys [J]. Acta Metallurgica Sinica, 2019, 55(9): 1145−1159. (in Chinese)

[5] EL-BAGOURY N. Ni based superalloy: Casting technology, metallurgy, development, properties and applications [J]. International Journal of Engineering Sciences & Research Technology, 2016, 5: 108−152.

[6] AMORE S, VALENZA F, GIURANNO D, NOVAKOVIC R, DALLA FONTANA G, BATTEZZATI L, RICCI E. Thermophysical properties of some Ni-based superalloys in the liquid state relevant for solidification processing [J]. Journal of Materials Science, 2016, 51: 1680−1691.

[7] MOOSAVY H N, ABOUTALEBI M R, SEYEDEIN S H, MAPELLI C. A solidification model for prediction of castability in the precipitation-strengthened nickel-based superalloys [J]. Journal of Materials Processing Technology, 2013, 213: 1875−1884.

[8] BAZHENOV V E, SAIDOV S S, TSELOVALNIK Y V, VOROPAEVA O O, PLISETSKAYA I V, TOKAR A A, BAZLOV A I, BAUTIN V A, KOMISSAROV A A, KOLTYGIN A V, BELOV V D. Comparison of castability, mechanical, and corrosion properties of Mg−Zn−Y−Zr alloys containing LPSO and W phases [J]. Transactions of Nonferrous Metals Society of China, 2021, 31(5): 1276−1290.

[9] JIE Zi-qi, ZHANG Jun, HUANG Tai-wen, SU Hai-jun, ZHANG Yan-bin, LIU Lin, FU Heng-zhi, Effects of boron and zirconium additions on the fluidity, microstructure and mechanical properties of IN718C superalloy [J]. Journal of Materials Research, 2016, 31: 3557−3566.

[10] BINCZYK F, CIEŚLA M, GRADOŃ P, FINDZIŃSKI R. Evaluation of casting shrinkage and liquid metal fluidity of IN-713C alloy [J]. Archives of Foundry Engineering, 2014, 14: 9−12.

[11] SZELIGA D. Manufacturing of thin-walled Ni-based superalloy castings using alternative thermal insulating module to control solidification [J]. Journal of Materials Processing Technology, 2020, 278: 116503.

[12] YIN F S, SUN X F, GUAN H R, HU Z Q. Effect of thermal history on the liquid structure of a cast nickel-base superalloy M963 [J]. Journal of Alloys and Compounds, 2004, 364: 225−228.

[13] TIMELLI G, CALIARI D. Effect of superheat and oxide inclusions on the fluidity of A356 alloy [J]. Materials Science Forum, 2017, 884: 71−80.

[14] KANYO J E, SCHAFFÖNER S, UWANYUZE R S, LEARY K S. An overview of ceramic molds for investment casting of nickel superalloys [J]. Journal of the European Ceramic Society, 2020, 40(15): 4955−4973.

[15] CHO Y H, KIM H W, LEE J M, KIM M S. A new approach to the design of a low Si-added Al−Si casting alloy for optimising thermal conductivity and fluidity [J]. Journal of Materials Science, 2015, 50(22): 7271−7281.
[16] MOTOYAMA Y, TOKUNAGA H, YOSHIDA M, MARUYAMA T, OKANE T. Measuring the interfacial heat transfer coefficient between flowing molten alloy and sand mold using fluidity tests [J]. Journal of Materials Processing Technology, 2020, 276: 116394.
[17] SHEVIDI A H, TAGHIABADI R, RAZAGHIAN A. Weibull analysis of effect of T6 heat treatment on fracture strength of AM60B magnesium alloy [J]. Transactions of Nonferrous Metals Society of China, 2018, 28(1): 20−29.
[18] FU Yu, WANG Han, ZHANG Chen, HAO Hai. Effects of minor Sr additions on the as-cast microstructure, fluidity and mechanical properties of Mg−4.2Zn−1.7RE−0.8Zr−0.2Ca (wt.%) alloy [J]. Materials Science and Engineering A, 2018, 723: 118−125.
[19] SHAH A W, HA S H, KIM B H, YOON Y O, LIM H K, KIM S K. Effect of Si addition on flow behavior in Al−Mg and Al−Mg−Si molten alloys [J]. Metallurgical and Materials Transactions A, 2020, 51: 6670−6678.
[20] SHIN J S, KO S H, KIM K T. Development and characterization of low-silicon cast aluminum alloys for thermal dissipation [J]. Journal of Alloys and Compounds, 2015, 644: 673−686.
[21] NIU Guo-dong, MAO Jian, WANG J. Effect of Ce addition on fluidity of casting aluminum alloy A356 [J]. Metallurgical and Materials Transactions A, 2019, 50: 5935−5944.
[22] WANG Fei-long, YIN Da-wei, LV Jing-wang, ZHANG Shan, MA Ming-zhen, ZHANG Xin-yu, LIU Ri-ping. Effect of cooling rate on fluidity and glass-forming ability of Zr-based amorphous alloys using different molds [J]. Journal of Materials Processing Technology, 2021, 292(1): 117051.
[23] PULIVARTI S R, BIRRU A K. Effect of mould coatings and pouring temperature on the fluidity of different thin cross-sections of A206 alloy by sand casting [J]. Transactions of the Indian Institute of Metals, 2018, 71: 1735−1745.
[24] MOTOYAMA Y, OZASA T, OKANE T. Accurate evaluation of copper alloy fluidity using automatic pouring equipment with improved pouring cup heat insulation [J]. Materials Transactions, 2017, 58: 629−634.
[25] MA Zhen, ZHANG Hua-rui, SONG Wei, WU Xiao-yan, JIA Li-na, ZHANG Hu. Pressure-driven mold filling model of aluminum alloy melt/semi-solid slurry based on rheological behavior [J]. Journal of Materials Science & Technology, 2020, 39: 14−21.
[26] HAN Q. A model correlating fluidity to alloy variables in hypoeutectic alloys [J]. Acta Materialia, 2022, 226: 117587.
[27] NIU Guo-dong, WANG Yu, ZHU Lang-jie, YE Jin-wen, MAO Jian. Fluidity of casting Al−Si series alloys for automotive light-weighting: A systematic review [J]. Materials Science and Technology, 2022, 38(13): 902−911.
[28] RAZA M, SVENNINGSSON R, IRWIN M, FÄGERSTRÖM B, JARFORS A E W. Effects of process related variations on fillablity simulation of thin-walled IN718 structures [J]. International Journal of Metalcasting, 2018, 12(3): 543−553.
[29] ZHOU Ye, MAO Ping-li, WANG Zhi, ZHOU Le, WANG Feng, LIU Zheng. Experimental investigation and simulation assessment on fluidity and hot tearing of Mg−Zn−Cu system alloys [J]. Journal of Materials Processing Technology, 2021, 297: 117259.
[30] ZHANG J, JIE Z Q, LIU M N, GUO M, LIU L. The fluidity test mold of superalloy and preparation method of test sample: China Patent, 202111615409.0 [P]. 2021−12−28.
[31] SUN Bao-de, WANG Jun, SHU Da. Precision forming technology of large superalloy castings for aircraft engines [M]. Shanghai: Shanghai Jiao Tong University Press, 2016. (in Chinese)

铸造高温合金通用的流动性测试模型及 IN718 和 IN939 流动性的比较

张 军[1]，介子奇[2]，刘淼楠[1]，郭 敏[1]

1. 西北工业大学 凝固技术国家重点实验室，西安 710072；
2. 西安工业大学 材料与化工学院，西安 710021

摘 要：设计高 10 mm、厚 3 mm 的高温合金螺旋流动性测试模型，以评估两种不同的镍基高温合金 IN718 和 IN939 的流动性。利用 JMatPro、差示扫描量热法和高温共聚焦激光扫描显微镜等方法进行对比分析，确定影响流动性的因素。结果表明，在相同的实验条件下，IN939 高温合金的流动性优于 IN718 高温合金。在相同温度条件下，IN939 高温合金熔体的黏度和表面张力远低于 IN718 高温合金，有利于提高熔体的流动性。此外，IN939 高温合金的液相温度和凝固区间均小于 IN718 高温合金。这种条件有助于延缓枝晶搭接，提高熔体流动性。

关键词：流动性；凝固区间；高温合金；表面张力；黏度

(Edited by Xiang-qun LI)